Advanced Design and Characterization of a Flat Panel Photobioreactor Equipped with a Customizable Light-Emitting Diode Lighting System

Advanced design and characterization of a flat panel photobioreactor equipped with a customizable LED lighting system.

Journal:	*ACS Sustainable Chemistry & Engineering*
Manuscript ID	sc-2023-05176q.R2
Manuscript Type:	Article
Date Submitted by the Author:	n/a
Complete List of Authors:	Carone, Michele; Politecnico di Torino, Department of Environment, Land and Infrastructure Engineering Frungieri, Graziano; Politecnico di Torino, Department of Applied Science and Technology Costamagna, Lorenzo; Politecnico di Torino, Department of Environment, Land and Infrastructure Engineering Zanetti , Mariachiara ; Politecnico di Torino, Department of Environment, Land and Infrastructure Engineerin Vanni, Marco; Politecnico di Torino, Dip. Scienza Applicata e Tecnologia Riggio, Vincenzo; Politecnico di Torino, Department of Environment, Land and Infrastructure Engineering

Advanced design and characterization of a flat panel photobioreactor equipped with a customizable LED lighting system.

Michele Carone[1], Graziano Frungieri[2], Lorenzo Costamagna[1], Mariachiara Zanetti[1], Marco Vanni[2], Vincenzo A. Riggio[1]*

1: Department of Environment, Land and Infrastructure Engineering, Politecnico di Torino, Corso Duca degli Abruzzi 24, 10129 Torino, Italy

2: Department of Applied Science and Technology, Institute of Chemical Engineering, Politecnico di Torino, Corso Duca degli Abruzzi 24, 10129 Torino, Italy

** Correspondence to Vincenzo A. Riggio at vincenzo.riggio@polito.it*

KEYWORDS

Flat Panel Photobioreactor, CFD simulation, Numerical tracer experiment, LED lighting, *Acutodesmus obliquus*, *Galdieria sulphuraria*.

ABSTRACT

Microalgae-based biorefinery processes are gaining particular importance to produce high-quality biomass and energy feedstock for several industrial markets. However, there are still several factors that contribute to poor yields of microalgae growth in current technologies. These include inadequate light management, inefficient gas exchange, limited control over temperature and pH, and susceptibility to contamination. Additionally, challenges associated with scalability and high operational costs of photobioreactors (PBR) further hinder the achievement of optimal yields in microalgae cultivation. This work presents a detailed characterization of a novel flat-panel PBR equipped with a tunable LED lighting system. A computational fluid dynamics (CFD) study was conducted to characterize in detail the equipment from the hydrodynamics point of view. CFD

results showed that the flow field has several peculiar features, such as vortices and a by-pass current, that can be expected to affect the light absorbance statistics, and the microalgae and nutrients spatial distributions. Considerations for both the system optimization and the modeling of its behavior during the operation were drawn. Additionally, two different microalgae strains, namely the green microalga *Acutodesmus obliquus* and the red extremophile *Galdieria sulphuraria*, each with specific growth parameters and spectra irradiation requirements, were successfully cultivated using tailored light spectra. The biomass concentrations and yields achieved (yields on light of 0.58 and 0.45 g mol_{ph}^{-1} for *A. obliquus* and *G. sulphuraria*, respectively) were consistent with currently reported productivities for both the species, highlighting the effectiveness of the adopted strategy for light management and the PBR overall design.

INTRODUCTION

Microalgae have become increasingly important as a source of biomass for various applications, including biofuels, animal feed, food, cosmetics, and dietary supplements. Compared to land

plants, microalgae are better at fixing carbon dioxide and converting solar energy into chemical energy, and they can grow faster and do not compete with arable land for cultivation [1–3]. Microalgal cultivation technologies are traditionally classified as open or closed systems (photobioreactors, PBRs). Open systems are cheaper to construct and manage, but they have limited biomass productivity due to poor mixing, low CO_2 mass transfer, and high risks of biological and chemical contamination [4,5]. Closed systems, on the other hand, allow for precise control of operating conditions and show higher biomass productivities, but they require higher capital and operating costs, as well as it is challenging to scale up their size while maintaining optimal culture and hydrodynamic parameters [6,7]. The yield of microalgae growth processes strongly depends on the design and operative conditions of the PBR. Dark and light zones typically coexist inside photobioreactors, i) because microalgal cultures are optically dense and hinder light penetration, and ii) because systems are often designed in such a way as to have microalgae experiencing alternate light cycles. This requires the microalgae to move between light and dark zones at a frequency that is high enough to support growth and not remain in dark fluid dead zones too long up to suffer a decrease in photosynthetic activity. As such, a PBR must be well-designed from the standpoint of hydrodynamics. CFD (computational fluid dynamics) simulations have emerged as

a low-cost and highly efficient strategy for designing microalgal growth equipment, as they can serve either the initial design stage of the PBR or the optimization of its operative conditions, eventually allowing one to reduce efforts on expensive and time-consuming experiments. CFD simulations can be used to obtain an accurate characterization of the flow field, possibly leading to the detection of a fluid dead zone, to get the statistics of shear stress and light absorbance along microalgae trajectories, or to detect the sedimentation and adhesion dynamics. By using CFD, Belolhav *et al.*, [8] for instance evaluated the hydrodynamics of a hybrid horizontal tubular PBR, showing that even at large flow velocities, low-velocity regions, prone to solid settling, can be expected. By a similar approach, Wang *et al.*, [9] and Hinterholz *et al.*, [10] developed and optimized the internal structure of a bioreactor by introducing inclined baffles which were seen to improve the swirling features of the flow. Through Lagrangian cell tracking combined with a solar radiation transfer model, Laifa and co-authors [11] related the overall growth rate to the broth velocity, as well as by applying CFD simulations, Zhang *et al.*, [12], studied the adhesion of cells and the biofilm growth on the walls of a bioreactor at varying surface roughness. Also, models aimed at coupling the bio-kinetics of microalgae growth and the equipment hydrodynamics have been devised [13–15] and seem to compare well with experimental data.

Managing light is another fundamental aspect in the design of photobioreactors, as it plays a crucial role in the growth and productivity of microalgae or cyanobacteria. Precise control of light parameters such as intensity, duration, and spectral composition is essential to optimize the desired physiological responses in these photosynthetic organisms and the energy supply. The provision of light energy can be achieved through natural sunlight or the use of artificial lamps. Utilizing sunlight as a light source offers the advantage of being free and readily available in abundance. However, it also presents certain drawbacks, including the presence of location-specific day/night cycles, unpredictable weather conditions, and seasonal variations. These fluctuations in irradiance levels can be mitigated by implementing artificial lighting. By employing continuous and controlled illumination, productivity can be enhanced, as biomass is not lost during night-time periods [16,17]. In the context of artificial lighting, the predominant choices are fluorescent tubes and light-emitting diodes (LEDs). LEDs offer numerous advantages compared to fluorescent tubes. They exhibit lower heat dissipation, resulting in reduced energy consumption, and possess a narrow emission spectrum, just to cite a few [18,19]. The utilization of light by phototrophic microalgae relies on their specific pigment composition, primarily chlorophylls, carotenoids, and phycobiliproteins, characterized by different absorption properties across distinct spectral

regions[20,21]. Furthermore, microalgae and their pigments are gaining increasing commercial interest as a source of natural high-value products [22,23]. The growth and metabolism of microalgae, including pigment content, can be influenced by the quality of light they receive, as determined by their spectral characteristics. Numerous studies have investigated the growth behavior and product formation of microalgae and cyanobacteria under various light conditions [18,21,24,25]. Nevertheless, most of those studies have been conducted with monochromatic or dichromatic illumination with fixed color ratios. Furthermore, such studies have been performed mostly at a lab scale in strictly controlled conditions, and to the authors' knowledge, no pilot-scale PBR equipped with multi-LEDs has been proposed so far.

The present work aims to propose a detailed characterization of a new semi-pilot scale prototype equipped with a multi-LEDs lighting engine. CFD simulations were carried out to characterize in detail the PBR's hydrodynamics. The study of the flow field in both the two constituent parts of the equipment, namely an alveolar flat panel and a mixing tank, was performed. CFD simulations were run in ANSYS Fluent 20.2 using a k-ε model for modeling turbulence, and numerical tracer experiments were run to infer the effect of the flow field on the species residence time and spatial distributions. Additionally, a description of the LED lighting engine is provided. The system

allows us to unpack the entire visible spectrum with the use of 10 wave lengths, produced by different LEDs, evenly distributed along the structure. The analysis of the incident light distribution along the entire surface of the flat panels is also provided and commented on. Finally, the efficiency of the system has been tested by carrying out batch tests with two commercially relevant microalgae, phylogenetically distant and with different pigment composition and abiotic conditions requirements. For each microalga, a specific light spectrum composition has been applied based on the oxygen evolution response as a performance indicator of photosynthesis from the cells exposed to the different wavelengths. The promising biomass yields obtained with both species reflect the potential and versatility of the PBR here described. The possibility of monitoring all growth parameters, as well as the tuning of light intensity and quality, make this system an excellent platform for the study and growth at a semi-pilot scale of several targeted algae or desired products. Various considerations and suggestions, especially related to the system's fluid dynamics, are provided, and will help to further improve the proposed technology and to evaluate its possible use in an industrial scenario, in which the application of energy-efficient technologies is nowadays a priority.

MATERIALS AND METHODS

The flat panel photobioreactor

The design, hydraulic, and mass transfer characteristics of the flat-panel PBR used in this work have been recently described in the literature [26]. Briefly, the PBR is composed of two parallel polycarbonate alveolar flat panels, each one partitioned into 28 alveoli for a total light-exposed surface of 1.5 m^2, and a truncated-cone shape tank where mixing and O_2 degassing is achieved. Liquid circulation occurs through a hydraulic circulator (ALPHA1 L - 45W, Grundfos, Denmark) located at the bottom of the mixing tank and upstream of the panels, allowing the culture to flow with positive pressure from the bottom to the top of the panels [Fig. 1A]. CO_2 injection (> 99.5% pure food grade) takes place between the bottom of the mixing tank and the hydraulic circulator, and the CO_2 flow rate is regulated by a thermal flow meter (Red-y smart controller GSC, Vögtlin Instruments GmbH Switzerland). The CO_2 flow rate is very small compared to that of the circulating liquid and, as a result, the gas dissolves almost immediately in the aqueous solution. Indeed, only few gas bubbles manage to reach the inlet of the tube panel. These bubbles are around 1 mm in size and dissolve completely in the first 10-20 cm of the tube. The PBR is equipped with a multi-probes system connected via a transductor to an integrated Programmable Logic Controller

(PLC) for both online and offline monitoring and control of cultivation parameters [26]. Compared to the PBR prototype reported in the above-mentioned study, the lighting hardware has been updated through the implementation of an own designed tunable-spectrum LEDs lighting engine directly managed by PLC, interposed between the two panels, instead of the more energy-consuming fluorescent tubes.

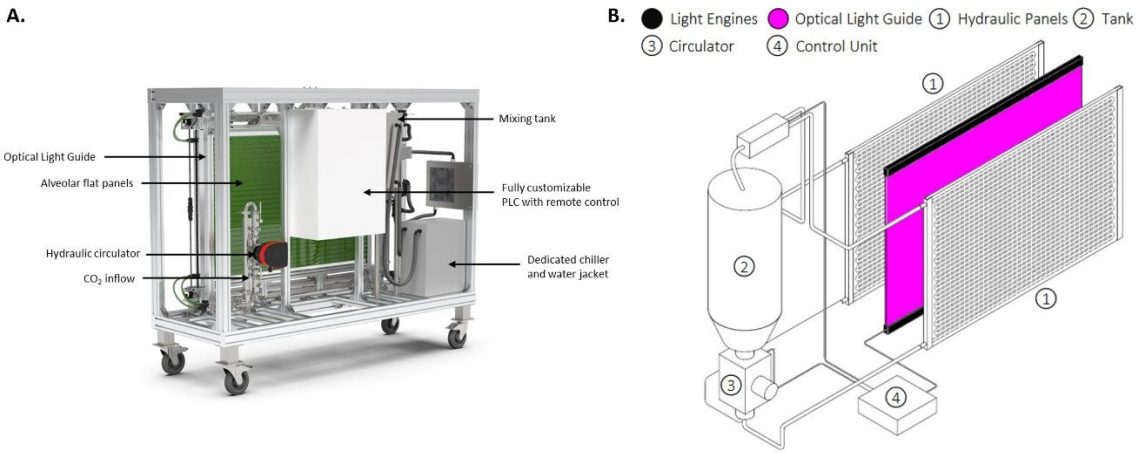

Figure 1: The alveolar flat-panel PBR. ***A.*** *3D isometric representation of the PBR.* ***B.*** *Schematic representation of the lighting engine. PLC: Programmable Logic Controller.*

LED lighting system

The lighting engine installed on the PBR is constituted by an innovative LED panel (patent number WO2020104895A1) engineered by MEG science (Milan, Italy), co-inventor of the system together with Arcobaleno Cooperativa Sociale (Turin, Italy) and the Polytechnic of Turin (Italy).

Excluding the mechanical and control components, two elements can be identified as the system's main core: the light engines and the optical guide [Fig. 1B]. The light engines are located at the upper and lower ends of the optical guide and are characterized by two water blocks that allow heat exchange between the electronic components (LEDs Printed Circuit Boards (PCBs)) and the external environment, using a forced water-cooled heat exchanger. This technical expedient serves to ensure operating temperatures below the safety junction temperature that characterizes each diode, increasing the efficiency and average lifetime of the individual LEDs. Each water block is equipped with 3 metal core LED PCBs, each populated by 10 LED clusters containing 12 power LEDs (Luxeon CZ Color Line, LUMILEDS, USA). The structure and configuration of this unit allow a spatially homogeneous distribution of the 10 discrete LEDs characterized by different peaks of dominant wavelength and 2 white light LEDs (not used in this work, as well as the Far-Red LEDs). The spectral range of the 10 dominant peak LEDs varies from 430 nm to 730 nm, while the two white LEDs are characterized respectively by a white with CCT (Correlated Color Temperature) 4000 K and CCT 5000 K. It is, therefore, possible to vary the quality and intensity of the light spectrum directly through the PLC. However, as indicated in Table S.1, this configuration is not normalized in terms of radiometric power, leading to a difference in the

furnished light intensity of the single wavelengths. This is due to the different spectral power distribution, and the related radiometric powers, of the considered LEDs, which nowadays constitutes a hardware limitation with red and blue LEDs considerably more efficient than other wavelengths. The optical guide is interposed between the two LED water blocks and ensures a homogeneous light distribution from the LEDs over the entire hydraulic panels' surfaces. The guide is made of polymethylmethacrylate (PMMA), with a length of 1500 mm and a height of 1120 mm, shaped in a 10 mm-thick sheet. Both the surfaces were laser-carved to obtain a pre-established pattern allowing the re-direction of light toward the hydraulic panels, assuring a certain degree of uniformity. Its geometry has been designed to allow an easy installation between the hydraulic panels in which the microalgae circulate and to reduce as much as possible the space between the emission source and the illuminated surfaces.

Computational Fluid Dynamics simulations setup

The CFD simulations were run using ANSYS FLUENT 20.2. The geometry of the reactor was created using ANSYS DesignModeler, whereas the meshes were created using the tool snappyHexMesh from OpenFOAM 5.0. Figure S.1 reports the geometry of the tank and some

detailed views of the mesh used for the simulations. The flow is fed to the mixing tank through a cascade flow, and it flows out via the bottom outlet tube. The cascade is reproduced as a vertical cylindric element of fluid with free slip at the lateral surface. The diameter of the inlet flow and the outlet tube are 2.5 and 2.6 cm, respectively. The top surface is the liquid-air interface, which stays at a constant level during the operation with a height, measured from the bottom of the tank, equal to 30 cm. Figure S.2 illustrates the geometry of the alveolar flat panel. The fluid enters the panel from the bottom right, and it flows to the left along the horizontal direction, then passes through the hole (magnified in the inset of Figure S.2) and reaches the upper channel, where it inverts its direction and moves to the next hole. The zigzagging motion generated by the sequence of 28 horizontal channels allows the fluid to spend sufficient time in the illuminated region of the equipment, but also generates a distribution of the residence times of the different elements of the liquid. CFD simulations were restricted to the portion of the system shown in green in the Figure S.2, since the fluid dynamics of the whole panel can be reconstructed by replicating such simulation at each turn.

The meshes of the tank and the flat panel are composed of approximately $1.0 \cdot 10^6$ and $1.3 \cdot 10^6$ hexahedral cells, respectively. The side of each cell is approximately equal to 1 mm. The mesh

quality was checked evaluating the cells' orthogonal quality, which was seen to be equal to 1 (on a scale from 0 to 1) in practically all the fluid domains. Grids of such resolution have shown to be able to accurately predict the velocity field, both in mixing tanks [27] and in ducts of rectangular cross section [28].

Since the CO_2 dissolves almost immediately in the circulating fluid, the process was modelled as single-phase flow. The fluid's properties and physical parameters were set by considering the culture medium as water. The inlet flow rates to the tank and the flat panel were set equal to 13.5 L min^{-1} and 6.75 L min^{-1}, respectively. The Reynolds number in the flat panel duct is about 8000 (based on the hydraulic diameter), well above the minimum value of 4000 required for the turbulence to occur [29]. The tank inlet duct has a Reynolds number just above 10000, making also this a turbulent flow, when feeding the tank inlet cascade.

A Reynolds-averaged approach for the computation of the system hydrodynamics was resorted. Under these conditions, the equation of fluid motion reads as in [Eq. (1)] and [Eq. (2)]:

$$\frac{\partial \overline{u}_i}{\partial x_i} = 0 \tag{1}$$

$$\rho\left(\frac{\partial \overline{u}_i}{\partial t}\right) + \frac{\partial}{\partial x_j}(\rho \overline{u}_i \overline{u}_j) = -\frac{\partial \overline{p}}{\partial x_i} + \frac{\partial}{\partial x_j}\left(\overline{\tau}_{ij} - \rho\overline{u_i' u_j'}\right) + \rho g_i \tag{2}$$

where $\bar{\tau}_{ij} = \mu\left(\frac{\partial \bar{u}_i}{\partial x_j} + \frac{\partial \bar{u}_j}{\partial x_i}\right)$ is the viscous stress tensor, μ the fluid viscosity, , $\bar{u}_i$ the velocity, $\bar{p}$ the fluid pressure, and ρ the fluid density, and where the bars indicate time-averaged quantities. The fluctuating component of the fluid velocity is denoted by u_i'. The Reynolds stress term $\rho\overline{u_i'u_j'}$ was modeled as in [Eq. (3)]:

$$-\rho\overline{u_i'u_j'} = \mu_t\left(\frac{\partial \bar{u}_i}{\partial x_j} + \frac{\partial \bar{u}_j}{\partial x_i}\right) \quad (3)$$

i.e., as proportional to the mean fluid velocity gradients and the turbulence viscosity μ_t. The two-equations $k-\varepsilon$ turbulence model was used for the closure of the set of equations. The turbulent kinetic energy k ($m^2\ s^{-2}$) and the rate of energy dissipation ε ($m^2\ s^{-3}$) were computed by solving the additional transport equations [Eq. (4), (5)]:

$$\rho\left(\frac{\partial k}{\partial t}\right) + \frac{\partial}{\partial x_i}(\rho k\bar{u}_i) = \frac{\partial}{\partial x_j}\left(\left(\mu + \frac{\mu_t}{\sigma_k}\right)\frac{\partial k}{\partial x_j}\right) + g_k - \rho\varepsilon \quad (4)$$

$$\rho\left(\frac{\partial \varepsilon}{\partial t}\right) + \frac{\partial}{\partial x_i}(\rho\varepsilon\bar{u}_i) = \frac{\partial}{\partial x_j}\left(\left(\mu + \frac{\mu_t}{\sigma_\varepsilon}\right)\frac{\partial \varepsilon}{\partial x_j}\right) + c_{1,\varepsilon}\frac{\varepsilon}{k}g_k - c_{2,\varepsilon}\rho\frac{\varepsilon^2}{k} \quad (5)$$

where the turbulent viscosity is given by $\mu_t = \rho c_\mu \frac{k^2}{\varepsilon}$, and where the set of $c_{1,\varepsilon}$, $c_{2,\varepsilon}$, c_μ, σ_k and σ_ε are as given in the standard implementation of the k-ε turbulence model of ANSYS Fluent.

No slip boundary conditions were imposed at all walls of the system, whereas a zero-stress condition was adopted for modeling the inlet cascade flow and the liquid-free surface of the tank.

The pressure-velocity coupling was achieved with the SIMPLE algorithm and a second-order upwind spatial discretization scheme was used to solve all the transport equations. In this work, the k-ε method used to describe turbulence is a Reynolds-Averaged Navier Stokes (RANS) technique that solves a time-averaged equation of motion, where the transient nature of turbulent fluctuations is absorbed by the Reynolds averaging. The averaged variables usually reach a stationary condition if the flow rate supplied does not vary over time, as is the case here. Hence, steady-state computations were performed. The simulations were iterated up to the point where the scales residuals of all variables between subsequent iterations stopped decreasing and reached an asymptotic value. This value was below 10^{-6} and, since additional iterations would not reduce the residuals any further, to the authors' opinion a condition where all the variables, including the local one, have attained convergence, is reached.

Due to the extremely special geometry of the system, direct comparisons with literature results are difficult to obtain. Modelling single-phase mixing tanks is a classic problem in chemical engineering, where reliable simulations are normally obtained using models and grid densities similar to those used in this work [30]. With regard to the duct, the simulations of this work were checked by comparing the prediction of the friction factor far away from the curves, where the

flow is fully developed, with the relationship reported by Schlichting (1979, chapter 20) [31], which is corroborated by the experimental data. However, the shape of the duct with U-curves of complex internal geometry makes it impossible to obtain full validation from literature.

It should be noted that a large number of experimental and modelling studies are available for motion in flat ducts of rectangular cross-section, but these are of little significance in the context of this work [32–36]. In fact, these studies often focus on the ability to predict the secondary flows triggered by the anisotropy of turbulence in straight ducts (Prandtl's secondary flow of the second kind). These, however, do not significantly alter the averaged profiles compared to canonical wall-bounded flows [37], being of modest intensity, with transverse velocities of the order of 1% of the axial ones. The k-ε method used in this work is unable to detect this particular type of secondary flow, which is triggered by the anisotropy of turbulence. It should be noted, however, that the relevant properties of the system, such as pressure drop and mixing in the panel, are dominated by the effects of the U-curves and the recirculation immediately following the curves, which is instead satisfactorily described by eddy-viscosity-based models such as the k-ε [38].

Microalgae-specific light spectra composition

The composition of the species-specific spectrum was based on the evaluation of the O_2 evolution response following cells' exposure to the individual wavelengths available on the PBR. More precisely, the cells of *A. obliquus* and *G. sulphuraria*, at a concentration of about 0.5 g L^{-1}, were directly exposed within the PBR at the individual wavelengths, each one adjusted to deliver about 30 μmol_{ph} m^{-2} s^{-1}, for 10 minutes after a 15-minute dark adaptation period and/or the time necessary for the O_2 concentration in the culture to be returned at equilibrium with the atmosphere. The averaged value of 30 μmol_{ph} m^{-2} s^{-1} was chosen according to the current upper range limit of some of the single wavelengths (*i.e.*, 499.5 and 520 nm). Oxygen evolution activity was recorded through the InPro 6000 Optical O_2 sensor located at the output of the panels. The ΔO_2 value recorded was then normalized by the light intensity for each wavelength. The final spectrum was built according to the wavelengths yielding net oxygen production, each of them set at a certain power percentage weighted for the corresponding yield of O_2.

Microalgae and cultivation conditions

Acutodesmus obliquus strain 276-3b, formally *Scenedesmus obliquus* (Turpin) Kützing, was obtained from the SAG Culture Collection of Algae (Göttingen, Germany), whereas *Galdieria*

sulphuraria strain 074W was kindly donated by Prof. Antonino Pollio (University of Naples, Italy). The PBR was inoculated with BG-11 medium [39] for *A. obliquus* or Allen medium [40] for *G. sulphuraria*, and microalgae cells for a total volume (V_{PBR}) of 60 L, corresponding to a surface area-to-volume ratio (S_f/V) of 50 m^{-1}, and an initial cell concentration of ≈ 0.25 g L^{-1} of dry weight. Each experiment was conducted in batch mode until the stationary phase was reached. The injection of CO_2 was carried out with a flow rate of 0.06 NL min^{-1}, keeping constant the CO_2 concentration threshold in the PBR at 25 mg L^{-1} for *A. obliquus* and 15 mg L^{-1} for *G. sulphuraria*, using the combination of solenoid valve and mass flow meter. The choice of key parameters for *A. obliquus*, such as temperature (23˚C ± 2) and pH (7.0-7.5), was done according to previous experiments performed within the same PBR structure equipped with fluorescent tubes, chosen among the most performing setups, as well as the spectrum-specific averaged photon flux density (*PFD*) on the panels' surface was set to 150 $\mu mol_{ph}\ m^{-2}\ s^{-1}$ (12.96 $mol_{ph}\ m^{-2}\ d^{-1}$), to have a fair comparison with the previously published results [26]. On the other hand, the red microalga *G. sulphuraria* is a polyextremophile organism that has been extensively studied due to its ability to survive at low pH (as low as 0.2 for some strains) [41], high temperatures (up to 57°C) and high osmotic pressure [42]. Therefore, the pH and temperature were adjusted to be 1.5-2.0 and 37.5˚C ± 2, respectively, according to several literature studies [43–46]. The spectrum-specific averaged PFD

was set to 125 μmol_{ph} m^{-2} s^{-1} since, according to its benthonic nature, *G. sulphuraria* is considered extremely photosensitive, usually growing at low light intensities [42,47], with light inhibition already occurring above 200 μmol_{ph} m^{-2} s^{-1} [41,45]. The culture medium temperature was controlled for both the microalgae using a thermostat (Lauda IN 250 XTW, Germany).

Biomass concentration measurements

Microalgae growth was gravimetrically quantified as dry biomass concentration as previously reported [26]. Briefly, 10-20 mL of microalgae culture were filtered using pre-weighted 1.5 µm pore size glass fiber filters (Hahnemühle, Germany), then dried using a thermobalance (MLS-N, Kern, Germany) until stable weight, and weighed with an analytical balance (Kern, Germany). The biomass volumetric productivity P_x [g L^{-1} d^{-1}] was then calculated as [Eq. (6)]:

$$P_x = \frac{X_{t+1} - X_t}{t_{+1} - t} \quad (6)$$

where X (t / $t+1$) is the biomass concentration [g L^{-1}] at the sampling time t / $t+1$ [d]. The volumetric productivity was then used to calculate the biomass yield on light $Y_{x/ph}$ [g mol_{ph}^{-1}] according to [41] [Eq. (7)]:

$$Y_{x/ph} = \frac{P_x \cdot V_{PBR}}{A_{PBR} \cdot PFD} \quad (7)$$

Where A_{PBR} [m^2] represents the total illuminated area (*i.e.*, 3 m^2 considering both the panels).

Radiance matrix

The uniformity of incident light on both panels' exposed surfaces was determined as previously reported [26]. Briefly, a matrix array was imposed on the artificial lighting system to fix, and homogeneously distribute, the *PFD* sampling points along the radiant surface. The *PFD* was determined by a calibrated Photosynthetic Active Radiation (PAR) spectroradiometer (PLA 20, Everfine, China). The measured *PFD* values were interpolated by the Linear model Poly22 of the Curve Fitting Tool of the software Matlab® to obtain a *PFD's* pattern for the whole exposed panel surface. The mean and minimum values of the obtained *PFD*'s matrix were then used to calculate the light uniformity coefficient (U_I[%]) as in Eq. (8):

$$U_I = \frac{I_{min}}{I_{mean}} \times 100 \quad (8)$$

where I_{min} is the *PFD* minimum value [$\mu mol_{ph}\ m^{-2}\ s^{-1}$] and I_{mean} is the *PFD* mean value [$\mu mol_{ph}\ m^{-2}\ s^{-1}$].

RESULTS AND DISCUSSION

CFD

Figure 2 reports a characterization of the flow field in both a 3D and a 2D view for three different cross sections. For each of those, a velocity magnitude contour plot, and a representation of the velocity field, as obtained by an arrow representation, were reported. Cross section 1 passes through the inlet of the tank, but not through the outlet which is instead included in cross section 2. Cross section 3 is instead parallel to the liquid-air-free surface of the tank. From the pictures, it is apparent that the inlet flow is slowed down upon impact on the free surface, and it is deviated towards the bulk of the tank by the inclined bottom walls. This is visible both in the velocity magnitude contour plot of cross section 1 and in the fluid path lines reported in the 3D view. It is also apparent that in the bulk of the mixing tank, the fluid undergoes a large recirculation motion with a vortical region that takes up almost completely the tank space, both in the vertical and horizontal directions. A lateral by-pass current traveling directly from the inlet to the outlet of the tank can also be observed. As it will be later discussed, these features of the flow field have a

relevant effect on the fluid residence time distributions in the tank. In cross section 2 the outlet flow is shown; here it is observed that the fluid flows out of the tank with a velocity that is close in magnitude to the inlet velocity, though with a velocity gradient that is unsymmetrical with respect to the tube centerline. This must be considered as a consequence of the lateral offset between the inlet and outlet flow.

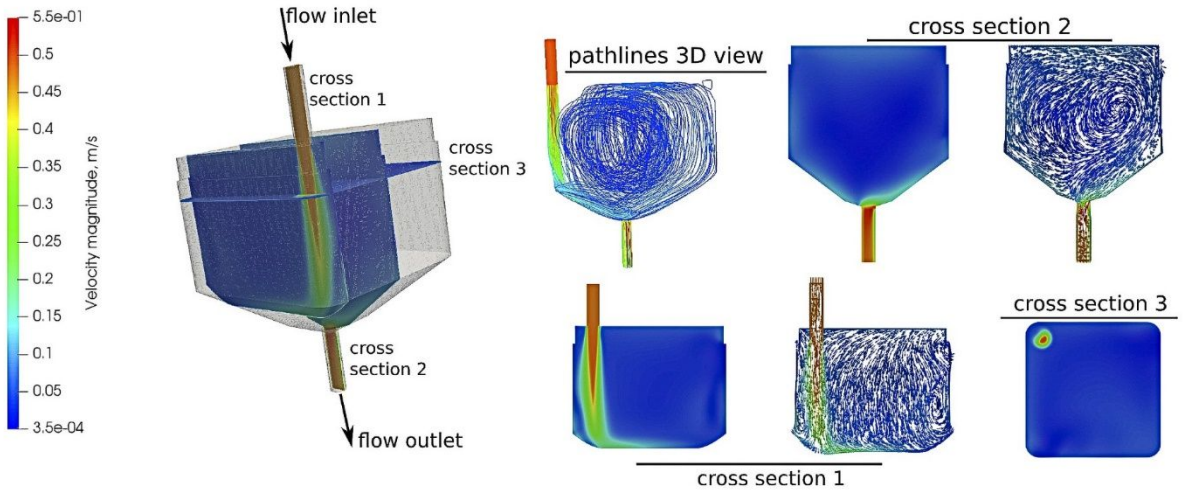

Figure 2: Visualization of the flow field in the mixing tank, by a contour plot representation of the velocity magnitude field and by fluid path lines. Three cross-sections are reported together with a 3D representation.

Concerning the panel, our simulations were limited to the green-shaded region of Figure S.2. As the horizontal channel connecting two subsequent turns is long enough for the flow to be fully developed, an identical replication of the flow configuration at every turn of the panel may be expected. This point was confirmed by checking the identity of the simulated velocity distribution at the midplanes of the two subsequent horizontal channels.

In Figure 3 only the portion of the flow field close to the passage hole was reported, as this is the region where the flow presents features of more worth. Figure 3A. illustrates the velocity field by a contour plot representation. It is seen here that the flow travels almost undisturbed until it reaches the passage hole, where it is accelerated reaching large velocities, particularly in the converging region of the hole close to the wall separating two subsequent channels. The flow field representations of Figure 3 B. and C. (streamlines and vectors of time-averaged velocity) make it also apparent that two vortical regions establish upstream and downstream of the passage hole. The first, visible in the bottom left corner, is a small, low-speed vortex, whereas the second, occurring downstream the passage hole, takes up a large vertical portion of the channel. However, this flow disturbance is seen to vanish completely at moderate distances from the passage hole.

From the inspection of the flow field just reported, it is apparent that a complex flow dynamics condition establishes in the two pieces of the equipment. To address this in some more detail, numerical tracer tests using non-reactive, dissolved species were performed. For the case of the tank, a step experiment was selected. Two non-interacting passive scalars were defined, one fed through the inlet flow at a constant concentration $c_{inlet} = c_0$, the second fed through the top liquid-free surface via a constant flux, such as a dissolved gas from the atmosphere. Within the tank, the

tracer is transported by the convective motion of the fluid, only, with the diffusive transport disregarded. This is done to assess the effect of the flow features on species' transport and to rule out the effect of species' molecular diffusion. Thus, the transport equation reads as [Eq. (9)]:

$$\frac{\partial c}{\partial t} + u_i \frac{\partial c}{\partial x_i} = 0 \qquad (9)$$

where c is the passive scalar concentration and where u_i is the fluid velocity as calculated by solving the fluid momentum transport equation. For both scalars, the outlet concentration *c(t)* as a function of time was measured.

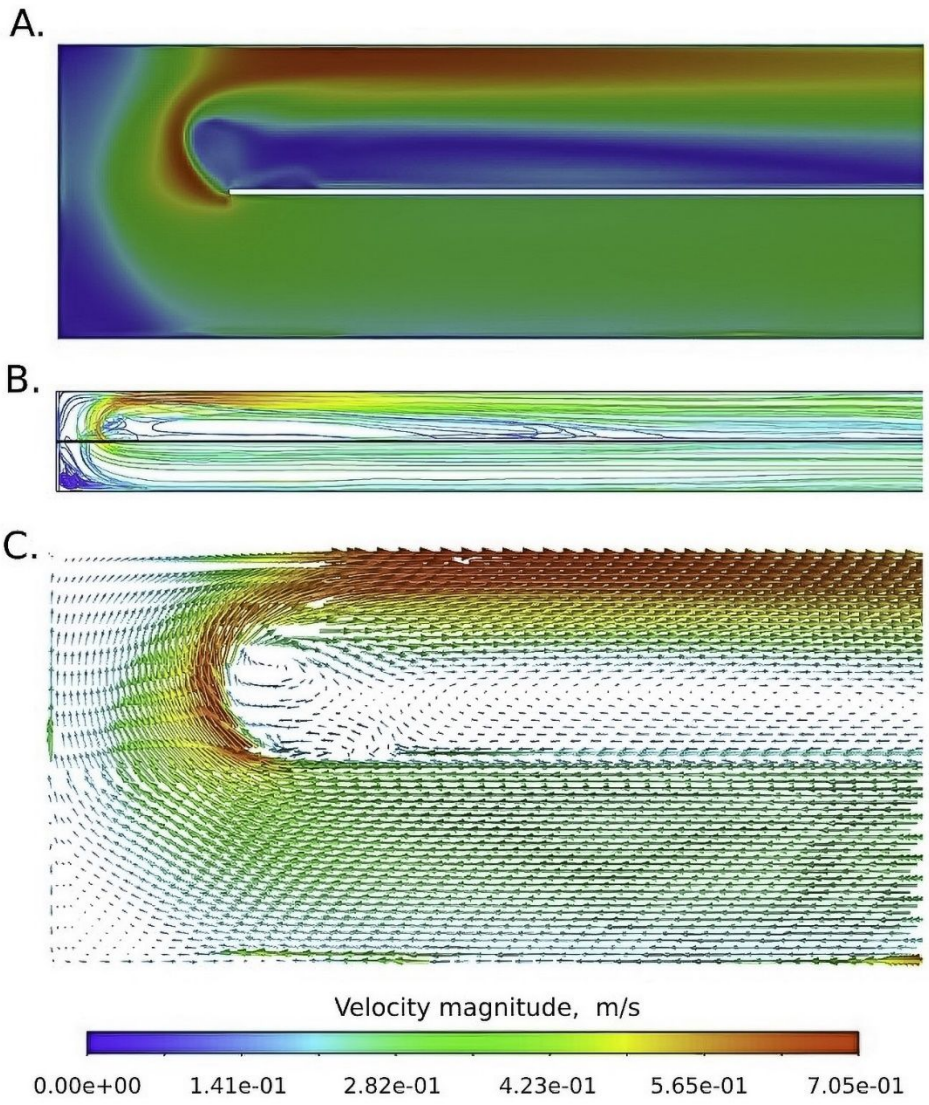

Figure 3: Visualization of the flow field in the flat panel. ***A.*** *Velocity magnitude contour plot.* ***B.*** *Fluid path lines.* ***C.*** *Arrow representation of the flow field. Each arrow is aligned with the local fluid velocity. The length and color of the arrows are set according to the velocity magnitude.*

The case of the release from the inlet is reported by the orange curve in Figure 4 together with a few snapshots of the spatial distribution of the tracer concentration. It is apparent that at the outlet the tracer concentration reaches, in a quite short time, a rather large value $(c \approx 0.32c_0)$ which

stays almost constant for approximately 25 s, and it then progressively approaches the asymptotic value ($c = c_0$). This response is the consequence of the inlet current that drags a large part of the tracer feed directly towards the bottom of the tank, from which it flows out practically by-passing the bulk of the fluid, as also visible in the concentration field snapshots at 10 and 100 s. The other part of the tracer feed flow is instead recirculated by the central vortex and spends a longer residence time in the tank. For comparison, the response of an ideal continuous stirred tank reactor is reported as a dotted line in the plot. The discrepancy between the two curves makes particularly apparent the by-pass phenomena just described.

The case of a uniform release from the tank-free surface is also reported in Figure 4. In this case, the concentration at large times reaches a lower value due to the dilution effect induced by the inlet flow. For this mode of release, no by-pass phenomena occur, and the system's dynamical behavior is very similar to the one that would be observed under perfectly mixed conditions. The uniform release from the liquid-free surface, together with the large vortical motion of the liquid bulk, distributes the tracer uniformly in the tank, making the outlet concentration increase more steadily until asymptotic conditions are reached, though with a delay compared to the perfectly mixed case.

The signals of the outlet concentration make it possible to calculate the mean residence time τ of the tracers for the two different modes of release as in [Eq. (10)]:

$$\tau = \frac{1}{c_0}\int_0^{c_0} t dc \tag{10}$$

This returned an average residence time equal to 86 s for the case of the release through the inlet flow, and 129 s for the case of the free surface release, with a difference compared to the average residence time under perfectly mixed conditions equal approximately to -8% and +37%, respectively.

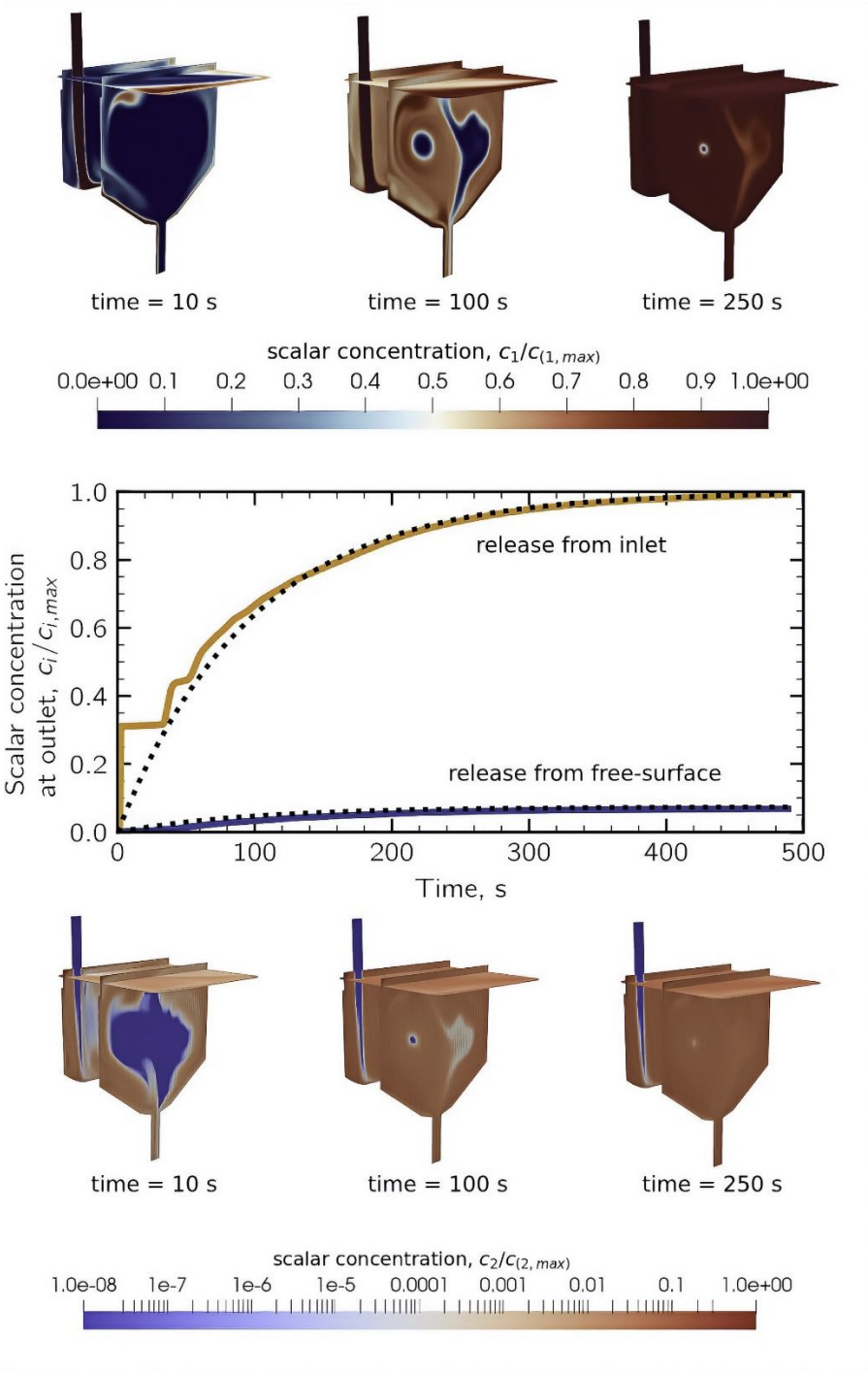

Figure 4: Results of the tracer experiments. Top) Concentration contour plot at three subsequent times for the case of a step release from the inlet. Centre) Concentration at the outlet as a function of time for the two modes of release. Bottom) Concentration contour plot at three subsequent times for the case of a step release from the liquid-free surface. The dotted lines report the outlet concentration that would be observed in perfectly mixed conditions.

Finally, in Figure 5 the distribution of the residence times in the flat panel, measured at the halfway of each channel, is reported. The measurement was done by an impulse experiment and by tracking tracer particles on the simulated domain. The results were extended to the whole flat panel by taking advantage of the system periodicity. It is seen that the residence time distribution of the particles is initially narrow, and it becomes wider after each channel. Finally, at the exit of the flat panel, three main peaks of decreasing height can be observed, approximately at 130 s, 140 s, and 165 s. This behavior is in line with what could be inferred from the analysis of the velocity field reported in Figure 3, where it could be observed that the channel arrangement induces the formation of two recirculation regions (one downstream and one upstream of each passage hole) and the occurrence of a large velocity region near the converging region of the hole. These flow field features make the particles to be redistributed longitudinally at each elbow and to display a rather wide residence time distribution at the flat panel exit.

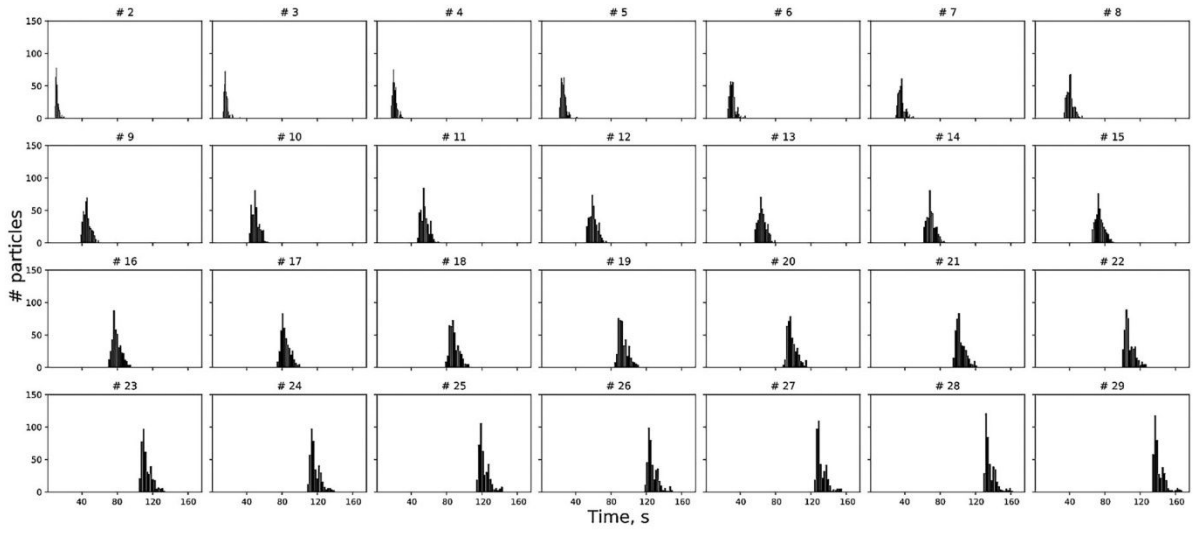

Figure 5: Residence time distributions measured at the halfway of the length of each channel of the alveolar flat panel as obtained by an impulse tracer experiment.

Light spectra composition

Although light absorption is wavelength-dependent, every PAR photon absorbed by the antennae can be used in the reaction centres to induce charge separation with the same efficiency, and results in an equal photosynthetic output. Nevertheless, the absorption bands of each pigment are different and, consequently, only certain wavelengths in the PAR region are effective for productive algal photosynthesis [48]. Red light, with a narrow spectrum of 600–700 nm, is usually reported as the optimal wavelength for the photosynthetic growth of most algal species [17,21,49,50].

This is primarily because the most abundant pigments in most species are chlorophylls which can more efficiently absorb red light compared to other light wavelengths [51]. However, due to its longer wavelength, the low-energy red light poorly penetrates high-density or deep cultures. Therefore, the cultures should be well mixed or kept at low concentrations under these light conditions [52]. On the other hand, blue light, with its shorter wavelength, has a higher probability to trigger photo-inhibition by striking the light-harvesting complexes due to its high energy content [50,53]. Overall, as reported in several works, the different wavelengths affect the cells' metabolism, by either enhancing the growth or the accumulation of specific compounds, acting differently according to the microalgae species [21,25,54–58]. The experiments described in this section aimed to assess, for each microalga used, the optimal conditions in terms of light quality. This ideal light composition was investigated by measuring the oxygen evolution response as a performance indicator of photosynthesis from the cells exposed to the different wavelengths directly within the PBR, and thus when cultivated on a large scale. In this way, the resulting spectra represent the combination of wavelengths, rather than using only monochromatic lights, weighted based on the algae's ability to trigger redox reactions within the chloroplast. Additionally, the possibility of qualitatively and quantitatively regulating the provided individual wavelengths may be a useful strategy to

investigate and minimize the energy consumption associated with the use of artificial light. The microalgae growth rates were then evaluated directly with the final ideal spectra, rather than testing the growth at each wavelength available in the PBR.

Figure 6 shows the ΔO_2 values obtained using the methodology described in the "Microalgae-specific light spectra composition" section. Not surprisingly, the blue and red spectral regions have the largest impact on photosynthesis in green algae (Fig. 6A.), due to the large number of molecules of chlorophyll a (*Chl a*) and chlorophyll b (*Chl b*) in the light-harvesting complexes (*LHCs*). From Fig 6A. It can be noted as the green (520nm) and orange (602 nm) lights do not lead to positive oxygen production. For the green light, the ΔO_2 is slightly negative, suggesting that the light at 520 nm induces electron transfer, but most probably the moles of photons given are not enough to reach the compensation point of photosynthesis. For instance, the light at 602 nm shows very negative ΔO_2 values, as there is a hardware limit linked to the fact that the photon flux at this wavelength is very small due to hardware limitations (around 6 $\mu mol_{ph}\ m^{-2}\ s^{-1}$ at the highest power). So, this suggests no photosynthetic electron transfer and thus only respiration occurring when applying only this light wavelength. For this reason, the ΔO_2 values that occurred

at 602 nm can be used as a reference for the cell's respiration. Fig. 6B. shows the correspondent spectrum used for *A. obliquus*.

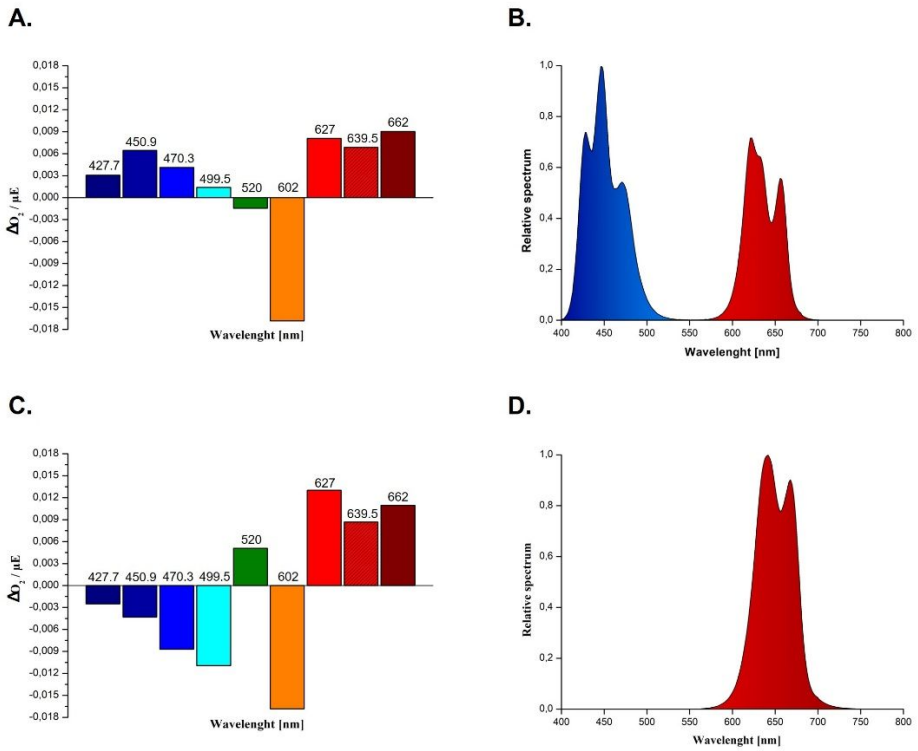

Figure 6: Light spectra customization. ***A.*** *Wavelength-specific normalized oxygen evolution response (ΔO_2 [mg L^{-1}] / µE [µmolph m^{-2} s^{-1}]) of A. obliquus.* ***B.*** *Resultant final spectrum employed for A. obliquus.* ***C.*** *Wavelength-specific normalized oxygen evolution response of G. sulphuraria.* ***D.*** *Resultant final spectrum employed for G. sulphuraria. (Kindly refer to section [2.4]). Graphs were produced with the software OriginPro8.5®.*

In contrast to green algae, red algae, as well as cyanobacteria, possess water-soluble Phycobilisomes (*PBS*) as major photosynthetic light-harvesting complexes. In G. *sulphuraria*, the PBSs are composed exclusively of allophycocyanin and (mainly) (C-) phycocyanin (*C-PC*) phycobiliproteins, with the *C-PC* having a single absorption maximum at ~ 620 nm [59]. Furthermore,

as widely reported in the literature, cyanobacteria and red algae possess low photosystem II / photosystem I (*PSII/PSI*) ratios, with the core complexes of *PSII* usually incorporating less *Chl a* than *PSI* cores [60,61]. Moreover, unlike green algae, *G. sulphuraria* also lacks *Chl b* and instead has zeaxanthin as its major xanthophyll [62]. In accordance with its photosynthetic apparatus, *G. sulphuraria* showed no positive oxygen production when illuminated with all the blue wavelengths [Fig. 6C.]. The wavelengths resulting in the highest positive ΔO_2 were 627 nm and 662 nm, and in less extent 639.5, being the first two closer to the maximal absorption peak of *C-PC* and *Chl a*, respectively. Although *Chl a* is not present around *PSII*, it provides the energy along the *C-PC* to *PSI*, therefore enhancing electron transfer between the two photosystems. Unlike *A. obliquus*, also green light (520nm) lead to positive oxygen evolution. Despite this, it has been decided to not include it in the correspondent spectrum since (Fig. 6D.), as previously reported, the cultivation process appears to not require a green or blue fraction to achieve optimal biomass productivity [21]. This would also reduce the energy consumption related to the artificial lighting system since in this prototype each LED is associated with a dedicated electric transformer. As for the light at 602nm, the same considerations for *A. obliquus* can be done, reflecting the need for adequate

hardware modifications if the effects on photosynthesis of this wavelength need to be further investigated.

Light homogeneity

Light availability in photoautotrophic microalgae cultivation is of primary importance for the overall process performance. Especially when employing artificial light, it is important to evaluate the light distribution along the photo-exposed surfaces to better characterize the amounts of photons and times at which microalgae cells are exposed. As previously investigated for a fluorescent tube light source, also in this work the light measurements on the exposed surfaces have been used to build up a radiant matrix for the two composed spectra used. The data were then computed as described in the "Radiance matrix" section, obtaining an averaged *PFD* of 150 μmol_{ph} m^{-2} s^{-1} and 125 μmol_{ph} m^{-2} s^{-1} for *A. obliquus* and *G. sulphuraria*, respectively, as well as a light uniformity coefficient U_I of 70% (Fig. 7A.) and 48% (Fig. 7B.). The considerable uniformity difference between the two spectra may be ascribed, as already addressed in the "LED lighting system" section, to the fact that the individual LEDs are distributed uniformly in clusters along the whole PCBs, but their distribution implies an unevenness from the emissive point of view. This is

most evident from Fig. 7B., where the composed spectrum for *G. sulphuraria* is characterized by only 3 wavelengths, and therefore by a lower resolution along the entire optical guide. This non-uniformity, with an important gradient of light intensity ranging from 250 to 50 μmol_{ph} m^{-2} s^{-1} along the surface of the hydraulic panels, may be overcome by changing the PCBs components, replacing the unintended wavelengths with a greater population of LEDs more uniform for each cluster. For the sake of simplicity, in this work, the averaged *PFD*s have been considered for the calculations of the biomass yields on light. Nevertheless, as pinpointed by Blanken et al. [63], the light distribution over the reactor surface has a significant influence on the growth rate, as high light will result in increased photosaturation. Further investigations on the growth kinetics with respect to the light distribution described in this section are currently ongoing.

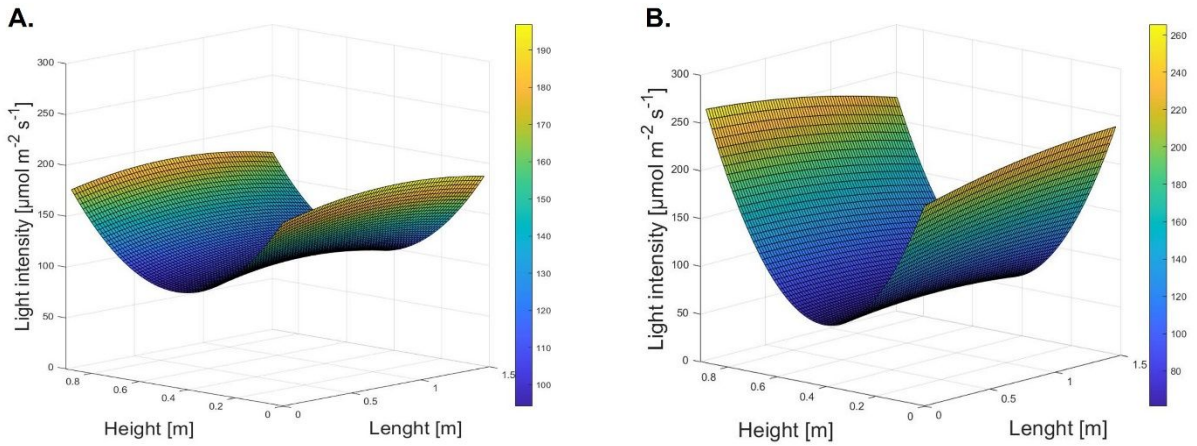

Figure 7: Graphical representation of the light intensity in a 3D space of the LEDs lighting source. PFDs measurements were interpolated by the Linear model Poly22 of the Curve Fitting Tool ($f(x,y) = p00 + p10*x + p01*y + p20*x^2 + p11*x*y + p02*y^2$ where x and y are the optical guide's length and height for the PFD sampling points, and p(n) the fitted coefficients) of the software

Matlab®. ***A.*** *Light intensity distribution for the light spectrum employed for A. obliquus. The goodness of fit: SSE = 320.3, R^2 = 0.972.* ***B.*** *Light intensity distribution for the light spectrum employed for G. sulphuraria. The goodness of fit: SSE = 70.2, R^2 = 0.995.*

Microalgae growth

In this study, the behaviour of PBR's fluid dynamics as well as the influence of the composed spectra on the biomass productivity of the two different microalgae (*A. obliquus*, *G. sulphuraria*) was investigated [26]. After 7 days of cultivation, the *A. obliquus* cells reached a final concentration of 2.305 g L^{-1} (Fig. 8A.). The analysis of the growth curves showed a mean daily volumetric productivity (P_x) of 0.295 g L^{-1} d^{-1} ± 0.03 (n = 3). The biomass yield on light energy was found to be on average 0.58 g mol_{ph}^{-1} during the exponential phase, a value between the highest found in the literature for several green microalgae [64,65], although continuous experiments should be performed to address consistent estimations of this value. Nevertheless, to the authors' opinion, there is ample room for improvement, especially considering that in this work the batch experiments were conducted with a relatively low averaged light intensity (150 μmol_{ph} m^{-2} s^{-1}). Overall, the results obtained in this work are slightly higher than what was found in the previous study conducted with fluorescent lights, where the average light intensity on the panels' surface

was found to be 120 μmol_{ph} m^{-2} s^{-1}. This confirms the suitability of using the composed optimized spectrum for *A. obliquus*.

The red microalga *Galdieria sulphuraria* is nowadays considered one of the most promising biotechnological platforms for food and feed applications, due to its peculiar polyextremophile characteristics, favouring a selective environment that prevents contaminations, as well as its high content of proteins, insoluble dietary fibers, and antioxidants [43,66]. Moreover, its amino acid profile is particularly noteworthy, as it contains a higher proportion of essential sulfur amino acids compared to *Chlorella*, *Spirulina*, and soybean protein [67].

In this work, it has been decided to assess the photoautotrophic growth of *G. sulphuraria* strain 074W, one of the most performant autotrophic strains [43], to show the versatility of the presented PBR to investigate and achieve high biomass growth even with extremophiles, far from common green microalgae.

After 16 days of cultivation, the cells reached a final concentration of 3.28 g L^{-1} (Fig. 8B.). The analysis of the growth curves showed a mean daily volumetric productivity P_x of 0.22 g L^{-1} d^{-1} ± 0.03 (n = 3). Although the observed P_x may seem quite low compared to other reported autotrophic batches [41,69], it is noteworthy pinpoint that the light intensity used is relatively low as well as, to

the authors' knowledge, this work is one of the few studies where *G. sulphuraria* growth was conducted at real scale. Indeed, the biomass yield on light energy was found to be on average 0.45 g mol_{ph}^{-1} during the exponential phase, a value in accordance with what has been found by Canelli and co-authors [70] in a 17 L annular column PBR (*G. sulphuraria* strains ACUF 064 and SAG 108.79), and close to the highest (0.5 – 0.65 g mol_{ph}^{-1}) reported for *G. sulphuraria* (ACUF 064 and 074G) grown in autotrophic conditions at lab-scale [41,67,69]. Taken together, the results obtained show the potential of the presented PBR prototype to achieve relatively high biomass concentrations, at a real scale, with more microalgae belonging to different phyla. Furthermore, the adopted strategy for the wavelength-specific spectra composition turned out to effectively achieve comparable yields on light obtained at the lab scale, especially considering *G. sulphuraria*. This aspect is relevant as, considering the cost of artificial lights, the possibility of choosing the optimal wavelengths according to the microorganisms' quantum requirements may strongly reduce the energy losses associated with, *e.g.*, blue-to-yellow light conversion in white LEDs, and the overall electric input. Nevertheless, the authors are in accordance with the fact that, due to the increase of the overall costs and the negative energy balances, the electrical energy required for microalgae cultivation employing artificial light should be generated as 'green' energy instead of

that derived from exploiting fossil fuels [17], or alternatively be used in compensation of sunlight to ensure a 24h production.

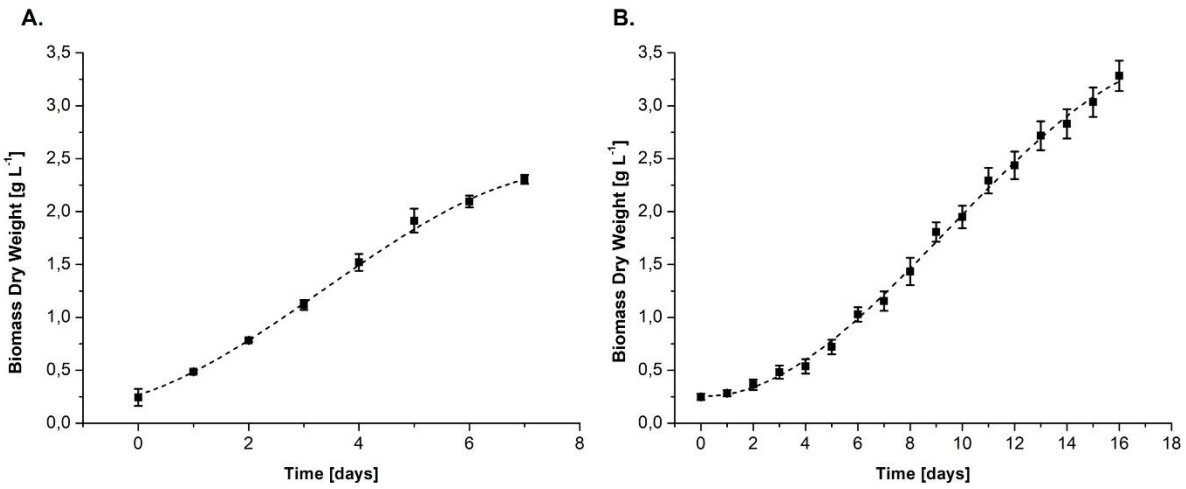

*Figure 8: Photoautotrophic batches. **A.** Biomass concentration of Acutodesmus obliquus in the flat panel photobioreactor. **B.** Biomass concentration of Galdieria sulphuraria in the flat panel photobioreactor. Squares represent the dry weight measurements ± standard deviation (n = 2 A. obliquus, n = 3 G. sulphuraria). The dotted lines represent the third-degree polynomial interpolation (R^2 = 0.999 A. obliquus, R^2 = 0.997 G. sulphuraria) obtained with the software OriginPro8.5®.*

CONCLUSION

In conclusion, the detailed characterization of a novel flat-panel PBR equipped with a LED lighting system is proposed. From the CFD analysis, it has been observed that the system hydrodynamics has several peculiar features which must be expected to determine the statistics of light and flow field sampling by the microalgae. In the mixing tank, two main regions of interest were observed: a vortex occupying almost completely the bulk of the tank, and a rather large lateral

by-pass current traveling directly from the inlet to the outlet, counting for approximately 30% of the inlet flow and having a short residence time compared to what is obtained under perfectly mixed conditions. Also, the flat panel was seen to have a peculiar feature: close to the passage hole between two subsequent channels, the fluid was accelerated and two vortical regions were observed, causing the axial dispersion of the particles and a distinctive behaviour of the distribution of the residence times. Overall, the CFD analysis returned several useful indications for the technical optimization of the system and put the basis for a few further studies. Among these, the use of internal baffles or deflectors of the fluid flow will be considered, as these can improve the mixing and mass transfer performance of the equipment.

The PBR has been equipped with a peculiar LED system capable of unpacking the entire visible spectrum. The possibility to dynamically change the light spectrum and intensity allows a high degree of customization of the cultivation process. This has been demonstrated by cultivating two completely different microalgae strains characterized by different growth parameters and spectral requirements. The biomass concentrations and yields achieved with both the strains, for which specific spectra were built, were perfectly in line with the data reported in the literature. These highlight the effectiveness of the adopted strategy for light management, which includes precise

control of the light intensity and wavelength, and showcase the high efficiencies achieved by the PBR, with still ample room for improvement also considering the low light intensities applied. The peculiar light management features would also open the investigation of wavelength-specific effects on biomass composition at a pilot scale. The PBR's hardware components, equipped with the multi-probes system – transductor - integrated PLC connections, make this prototype already suitable for remote monitoring and control of cultivation parameters to incorporate the Internet of Things (IoT). This aspect is becoming relevant as both academic research and industry are gradually moving towards process automation and remote operation. Future research will focus on advance optimizing the PBR design and exploring the economic viability of scaling up the system for commercial production.

ASSOCIATED CONTENT

Supporting Information. Table S.1: LEDs technical specifications extrapolated from the producers' technical sheet; Figure S.1: The geometry of the tank and some detailed views of the

mesh used for the simulations; Figure S.2: The geometry of the alveolar flat panels with details on the hydraulic direction change section.

AUTHOR INFORMATION

Corresponding Author

*E-mail: vincenzo.riggio@polito.it

Author Contributions

M.C.: Conceptualization, Investigation, Formal analysis, Methodology, Data curation, Writing – original draft. G.F.: Investigation, Formal analysis, Methodology, Data curation, Writing – original draft. L.C.: Investigation, Formal analysis. M.Z.: Formal analysis, Writing – review & editing, Funding acquisition. M.V.: Formal analysis, Methodology, Writing – review & editing. V.A.R.: Conceptualization, Investigation, Formal analysis, Data curation, Writing – review & editing, Project administration, Funding acquisition.

Funding Sources

This publication is part of the project NODES which has received funding from the MUR – M4C2 1.5 of PNRR funded by the European Union - NextGenerationEU (Grant agreement no. ECS00000036).

ACKNOWLEDGMENT

The authors dedicate this manuscript to the memory of Dr. Graziano Frungieri, who passed away during the revision process. The authors are also grateful to Piero Santoro from MEG Science (Milan, Italy) for the realization of the LED lighting system, Andrea Occhipinti from Abel Nutraceuticals (Turin, Italy), Arcobaleno Cooperativa Sociale (Turin, Italy) in the person of F. Passarelli and F. De Bernardi for their technical support.

REFERENCES

(1) Carlsson, A. S.; van Beilen, J. B.; Möller, R.; Clayton, D. *Micro- and Macro-Algae: Utility for Industrial Applications*; Outputs from the EPOBIO Project. CPL Press, Berks., 2007.

(2) Goli, A.; Shamiri, A.; Talaiekhozani, A.; Eshtiaghi, N.; Aghamohammadi, N.; Aroua, M. K. An Overview of Biological Processes and Their Potential for CO2 Capture. *Journal of Environmental Management*. Academic Press December 1, 2016, pp 41–58. https://doi.org/10.1016/j.jenvman.2016.08.054.

(3) Rosenberg, J. N.; Mathias, A.; Korth, K.; Betenbaugh, M. J.; Oyler, G. A. Microalgal Biomass Production and Carbon Dioxide Sequestration from an Integrated Ethanol Biorefinery in Iowa: A Technical Appraisal and Economic Feasibility Evaluation. *Biomass Bioenergy* **2011**, *35* (9), 3865–3876. https://doi.org/10.1016/j.biombioe.2011.05.014.

(4) Benemann, J. Microalgae for Biofuels and Animal Feeds. *Energies (Basel)* **2013**, *6* (11), 5869–5886. https://doi.org/10.3390/en6115869.

(5) Acién, F. G.; Molina, E.; Reis, A.; Torzillo, G.; Zittelli, G. C.; Sepúlveda, C.; Masojídek, J. *Photobioreactors for the Production of Microalgae*; 2017. https://doi.org/10.1016/B978-0-08-101023-5.00001-7.

(6) Adesanya, V. O.; Cadena, E.; Scott, S. A.; Smith, A. G. Life Cycle Assessment on Microalgal Biodiesel Production Using a Hybrid Cultivation System. *Bioresour Technol* **2014**, *163*, 343–355. https://doi.org/10.1016/j.biortech.2014.04.051.

(7) Norsker, N. H.; Barbosa, M. J.; Vermuë, M. H.; Wijffels, R. H. Microalgal Production - A Close Look at the Economics. *Biotechnol Adv* **2011**, *29* (1), 24–27. https://doi.org/10.1016/j.biotechadv.2010.08.005.

(8) Belohlav, V.; Uggetti, E.; García, J.; Jirout, T.; Kratky, L.; Díez-Montero, R. Assessment of Hydrodynamics Based on Computational Fluid Dynamics to Optimize the Operation of Hybrid Tubular Photobioreactors. *J Environ Chem Eng* **2021**, *9* (5). https://doi.org/10.1016/j.jece.2021.105768.

(9) Wang, L.; Wang, Q.; Zhao, R.; Tao, Y.; Ying, K. Z.; Mao, X. Z. Novel Flat-Plate Photobioreactor with Inclined Baffles and Internal Structure Optimization to Improve Light Regime Performance. *ACS Sustain Chem Eng* **2021**, *9* (4), 1550–1558. https://doi.org/10.1021/acssuschemeng.0c06109.

(10) Hinterholz, C. L.; Trigueros, D. E. G.; Módenes, A. N.; Borba, C. E.; Scheufele, F. B.; Schuelter, A. R.; Kroumov, A. D. Computational Fluid Dynamics Applied for the Improvement of a Flat-Plate Photobioreactor towards High-Density Microalgae Cultures. *Biochem Eng J* **2019**, *151*. https://doi.org/10.1016/j.bej.2019.107257.

(11) Laifa, R.; Morchain, J.; Barna, L.; Guiraud, P. A Numerical Framework to Predict the Performances of a Tubular Photobioreactor from Operating and Sunlight Conditions. *Algal Res* **2021**, *60* (102550).

(12) Zhang, Q.; Yu, Z.; Jin, S.; Liu, C.; Li, Y.; Guo, D.; Hu, M.; Ruan, R.; Liu, Y. Role of Surface Roughness in the Algal Short-Term Cell Adhesion and Long-Term Biofilm Cultivation under Dynamic Flow Condition. *Algal Res* **2020**, *46*. https://doi.org/10.1016/j.algal.2019.101787.

(13) Frungieri, G.; Carone, M.; Riggio, V.; Buffo, A.; Vanni, M.; Zanetti, M. Numerical Modelling of a Lab-Scale Reactor for Microalgae Growth. *Chem Eng Trans* **2022**, *92*, 127–132. https://doi.org/10.3303/CET2292022.

(14) Fernández del Olmo, P.; Acién, F. G.; Fernández-Sevilla, J. M. Productivity Analysis in Tubular Photobioreactors Using a Dynamic Photosynthesis Model Coupled to Computational Fluid Dynamics Particle Tracking. *Bioresour Technol* **2022**, *344*. https://doi.org/10.1016/j.biortech.2021.126277.

(15) Anye Cho, B.; Grobler, E.; William McClelland Pott, R.; Antonio del Río Chanona, E.; Zhang, D. A CFD Coupled Photo-Bioreactive Transport Modelling of Tubular Photobioreactor Mixed by Peristaltic Pump. *Chem Eng Sci* **2023**, *270*. https://doi.org/10.1016/j.ces.2023.118525.

(16) Cuaresma, M.; Janssen, M.; Vílchez, C.; Wijffels, R. H. Productivity of Chlorella Sorokiniana in a Short Light-Path (SLP) Panel Photobioreactor under High Irradiance. *Biotechnol Bioeng* **2009**, *104* (2), 352–359. https://doi.org/10.1002/bit.22394.

(17) Blanken, W.; Cuaresma, M.; Wijffels, R. H.; Janssen, M. Cultivation of Microalgae on Artificial Light Comes at a Cost. *Algal Research*. October 2013, pp 333–340. https://doi.org/10.1016/j.algal.2013.09.004.

(18) Schulze, P. S. C.; Barreira, L. A.; Pereira, H. G. C.; Perales, J. A.; Varela, J. C. S. Light Emitting Diodes (LEDs) Applied to Microalgal Production. *Trends in Biotechnology*. Elsevier Ltd 2014, pp 422–430. https://doi.org/10.1016/j.tibtech.2014.06.001.

(19) Radzun, K. A.; Wolf, J.; Jakob, G.; Zhang, E.; Stephens, E.; Ross, I.; Hankamer, B. Automated Nutrient Screening System Enables High-Throughput Optimisation of Microalgae Production Conditions. *Biotechnol Biofuels* **2015**, *8* (1). https://doi.org/10.1186/s13068-015-0238-7.

(20) Carvalho, A. P.; Silva, S. O.; Baptista, J. M.; Malcata, F. X. Light Requirements in Microalgal Photobioreactors: An Overview of Biophotonic Aspects. *Applied Microbiology and Biotechnology*. March 2011, pp 1275–1288. https://doi.org/10.1007/s00253-010-3047-8.

(21) Baer, S.; Heining, M.; Schwerna, P.; Buchholz, R.; Hübner, H. Optimization of Spectral Light Quality for Growth and Product Formation in Different Microalgae Using a Continuous Photobioreactor. *Algal Res* **2016**, *14*, 109–115. https://doi.org/10.1016/j.algal.2016.01.011.

(22) Borowitzka, M. A. High-Value Products from Microalgae-Their Development and Commercialisation. *Journal of Applied Phycology*. June 2013, pp 743–756. https://doi.org/10.1007/s10811-013-9983-9.

(23) Koller, M.; Muhr, A.; Braunegg, G. Microalgae as Versatile Cellular Factories for Valued Products. *Algal Research*. Elsevier B.V. October 1, 2014, pp 52–63. https://doi.org/10.1016/j.algal.2014.09.002.

(24) Vadiveloo, A.; Moheimani, N. R.; Cosgrove, J. J.; Bahri, P. A.; Parlevliet, D. Effect of Different Light Spectra on the Growth and Productivity of Acclimated Nannochloropsis Sp. (Eustigmatophyceae). *Algal Res* **2015**, *8*, 121–127. https://doi.org/10.1016/j.algal.2015.02.001.

(25) Han, P. P.; Shen, S. G.; Wang, H. Y.; Sun, Y.; Dai, Y. J.; Jia, S. R. Comparative Metabolomic Analysis of the Effects of Light Quality on Polysaccharide Production of Cyanobacterium Nostoc Flagelliforme. *Algal Res* **2015**, *9*, 143–150. https://doi.org/10.1016/j.algal.2015.02.019.

(26) Carone, M.; Alpe, D.; Costantino, V.; Derossi, C.; Occhipinti, A.; Zanetti, M.; Riggio, V. A. Design and Characterization of a New Pressurized Flat Panel Photobioreactor for

Microalgae Cultivation and CO2 Bio-Fixation. *Chemosphere* **2022**, *307*. https://doi.org/10.1016/j.chemosphere.2022.135755.

(27) Maluta, F.; Buffo, A.; Marchisio, D.; Montante, G.; Paglianti, A.; Vanni, M. Effect of Turbulent Kinetic Energy Dissipation Rate on the Prediction of Droplet Size Distribution in Stirred Tanks. *International Journal of Multiphase Flow* **2021**, *136*, 103547. https://doi.org/10.1016/j.ijmultiphaseflow.2020.103547.

(28) Faria, R.; Ferreira, A. D.; Lopes, A. M. G.; Sousa, A. C. M. Modeling of Turbulent Flows in Rectangular Ducts Using Openfoam®. In *OpenFOAM - Selected Papers of the 11th Workshop*; Springer, 2019; pp 325–340. https://doi.org/10.1007/978-3-319-60846-4_24.

(29) White, F. M. *Viscous Fluid Flow*, 3rd ed.; McGraw-Hill Higher Education, 2006.

(30) Ranade, V. V. *Computational Flow Modeling for Chemical Reactor Engineering*, 1st ed.; Academic Press, 2001.

(31) Schlichting, H. *Boundary Layer Theory*, 7th ed.; McGraw-Hill, 1979.

(32) Hinze, J. O. Experimental Investigation on Secondary Currents in the Turbulent Flow through a Straight Conduit. *Applied Scientific Research* **1973**, *28* (1), 453–465. https://doi.org/10.1007/BF00413083.

(33) Melling, A.; Whitelaw, J. H. Turbulent Flow in a Rectangular Duct. *J Fluid Mech* **1976**, *78* (2), 289–315. https://doi.org/10.1017/S0022112076002450.

(34) Bradshaw, P. Turbulent Secondary Flows. *Annu Rev Fluid Mech* **1987**, *19* (1), 53–74. https://doi.org/10.1146/annurev.fl.19.010187.000413.

(35) Yao, J.; Zhao, Y.; Fairweather, M. Numerical Simulation of Turbulent Flow through a Straight Square Duct. *Appl Therm Eng* **2015**, *91*, 800–811. https://doi.org/10.1016/j.applthermaleng.2015.08.065.

(36) Stankovic, B.; Belosevic, S.; Crnomarkovic, N.; Stojanovic, A.; Tomanovic, I.; Milicevic, A. Specific Aspects of Turbulent Flow in Rectangular Ducts. *Thermal Science* **2017**, *21* (suppl. 3), 663–678. https://doi.org/10.2298/TSCI160201189S.

(37) Orlandi, P.; Pirozzoli, S. Transitional and Turbulent Flows in Rectangular Ducts: Budgets and Projection in Principal Mean Strain Axes. *Journal of Turbulence* **2020**, *21* (5–6), 286–310. https://doi.org/10.1080/14685248.2020.1779276.

(38) Pope, S. B. *Turbulent Flows*; Cambridge University Press, 2000.

(39) Stanier, R. Y.; Kunisawa, R.; Mandel, M.; Cohen-Bazire, G. Purification and Properties of Unicellular Blue-Green Algae (Order Chroococcales). *Bacteriol Rev* **1971**, *35* (2), 171–205. https://doi.org/10.1128/mmbr.35.2.171-205.1971.

(40) Allen, M. B. Studies with Cyanidium Caldarium, an Anomalously Pigmented Chlorophyte. *Arch Mikrobiol* **1959**, *32*, 270–277.

(41) Abiusi, F.; Trompetter, E.; Hoenink, H.; Wijffels, R. H.; Janssen, M. Autotrophic and Mixotrophic Biomass Production of the Acidophilic Galdieria Sulphuraria ACUF 64. *Algal Res* **2021**, *60*. https://doi.org/10.1016/j.algal.2021.102513.

(42) Pinto, G.; Ciniglia, C.; Cascone, C.; Pollio, A. A. Species Composition of Cyanidiales Assemblages in Pisciarelli (Campi Flegrei, Italy) and Description of Galdieria Phlegrea SP. NOV. In *Algae and Cyanobacteria in Extreme Environments. Cellular Origin, Life in Extreme Habitats and Astrobiology.*; Seckbach, J., Ed.; Springer: Dordrecht, 2007; Vol. 11, pp 487–502. https://doi.org/https://doi.org/10.1007/978-1-4020-6112-7_26.

(43) Graziani, G.; Schiavo, S.; Nicolai, M. A.; Buono, S.; Fogliano, V.; Pinto, G.; Pollio, A. Microalgae as Human Food: Chemical and Nutritional Characteristics of the Thermo-Acidophilic Microalga Galdieria Sulphuraria. *Food Funct* **2013**, *4* (1), 144–152. https://doi.org/10.1039/c2fo30198a.

(44) Oesterhelt, C.; Schmälzlin, E.; Schmitt, J. M.; Lokstein, H. Regulation of Photosynthesis in the Unicellular Acidophilic Red Alga Galdieria Sulphuraria. *Plant Journal* **2007**, *51* (3), 500–511. https://doi.org/10.1111/j.1365-313X.2007.03159.x.

(45) Sloth, J. K.; Wiebe, M. G.; Eriksen, N. T. Accumulation of Phycocyanin in Heterotrophic and Mixotrophic Cultures of the Acidophilic Red Alga Galdieria Sulphuraria. *Enzyme Microb Technol* **2006**, *38* (1–2), 168–175. https://doi.org/10.1016/j.enzmictec.2005.05.010.

(46) Selvaratnam, T.; Pegallapati, A. K.; Montelya, F.; Rodriguez, G.; Nirmalakhandan, N. Bioresource Technology Evaluation of a Thermo-Tolerant Acidophilic Alga , Galdieria Sulphuraria , for Nutrient Removal from Urban Wastewaters. *Bioresour Technol* **2014**, *156*, 395–399. https://doi.org/10.1016/j.biortech.2014.01.075.

(47) Carbone, D. A.; Olivieri, G.; Pollio, A.; Melkonian, M. Comparison of Galdieria Growth and Photosynthetic Activity in Different Culture Systems. *AMB Express* **2020**, *10* (1). https://doi.org/10.1186/s13568-020-01110-7.

(48) Atta, M.; Idris, A.; Bukhari, A.; Wahidin, S. Intensity of Blue LED Light: A Potential Stimulus for Biomass and Lipid Content in Fresh Water Microalgae Chlorella Vulgaris. *Bioresour Technol* **2013**, *148*, 373–378. https://doi.org/10.1016/j.biortech.2013.08.162.

(49) Baba, M.; Kikuta, F.; Suzuki, I.; Watanabe, M. M.; Shiraiwa, Y. Wavelength Specificity of Growth, Photosynthesis, and Hydrocarbon Production in the Oil-Producing Green Alga Botryococcus Braunii. *Bioresour Technol* **2012**, *109*, 266–270. https://doi.org/10.1016/j.biortech.2011.05.059.

(50) Wang, S. K.; Stiles, A. R.; Guo, C.; Liu, C. Z. Microalgae Cultivation in Photobioreactors: An Overview of Light Characteristics. *Engineering in Life Sciences*. Wiley-VCH Verlag November 1, 2014, pp 550–559. https://doi.org/10.1002/elsc.201300170.

(51) Matthijs, H. C. P.; Balke, H.; Van Hes, U. M.; A Kroon, B. M.; Mur, L. R.; Binot, R. A. *Application of Light-Emitting Diodes in Bioreactors: Flashing Light Effects and Energy Economy in Algal Culture (Ch/Ore//a Pyrenoidosa)*; John Wiley & Sons, Inc, 1996; Vol. 50.

(52) Mohsenpour, S. F.; Willoughby, N. Luminescent Photobioreactor Design for Improved Algal Growth and Photosynthetic Pigment Production through Spectral Conversion of Light. *Bioresour Technol* **2013**, *142*, 147–153. https://doi.org/10.1016/j.biortech.2013.05.024.

(53) Das, P.; Lei, W.; Aziz, S. S.; Obbard, J. P. Enhanced Algae Growth in Both Phototrophic and Mixotrophic Culture under Blue Light. *Bioresour Technol* **2011**, *102* (4), 3883–3887. https://doi.org/10.1016/j.biortech.2010.11.102.

(54) Teo, C. L.; Atta, M.; Bukhari, A.; Taisir, M.; Yusuf, A. M.; Idris, A. Enhancing Growth and Lipid Production of Marine Microalgae for Biodiesel Production via the Use of Different LED Wavelengths. *Bioresour Technol* **2014**, *162*, 38–44. https://doi.org/10.1016/j.biortech.2014.03.113.

(55) Niizawa, I.; Leonardi, R. J.; Irazoqui, H. A.; Heinrich, J. M. Light Wavelength Distribution Effects on the Growth Rate of Scenedesmus Quadricauda. *Biochem Eng J* **2017**, *126*, 126–134. https://doi.org/10.1016/j.bej.2016.09.006.

(56) Leonardi, R. J.; Niizawa, I.; Irazoqui, H. A.; Heinrich, J. M. Modeling and Simulation of the Influence of Fractions of Blue and Red Light on the Growth of the Microalga Scenedesmus Quadricauda. *Biochem Eng J* **2018**, *129*, 16–25. https://doi.org/10.1016/j.bej.2017.10.014.

(57) Kula, M.; Rys, M.; Mozdzeń, K.; Skoczowski, A. Metabolic Activity, the Chemical Composition of Biomass and Photosynthetic Activity of Chlorella Vulgaris under Different Light Spectra in Photobioreactors. *Eng Life Sci* **2014**, *14* (1), 57–67. https://doi.org/10.1002/elsc.201200184.

(58) Dikicioglu, D.; Wood, V.; Rutherford, K. M.; McDowall, M. D.; Oliver, S. G. Improving Functional Annotation for Industrial Microbes: A Case Study with Pichia Pastoris. *Trends in Biotechnology*. Elsevier Ltd 2014, pp 396–399. https://doi.org/10.1016/j.tibtech.2014.05.003.

(59) Eriksen, N. T. Production of Phycocyanin - A Pigment with Applications in Biology, Biotechnology, Foods and Medicine. *Applied Microbiology and Biotechnology*. August 2008, pp 1–14. https://doi.org/10.1007/s00253-008-1542-y.

(60) Jordan, P.; Fromme[2], P.; Witt[2], H. T.; Klukas, O.; Saenger, W.; Krauû, N. Three-Dimensional Structure of Cyanobacterial Photosystem I at 2.5 A Ê Resolution. *Nature* **2001**, *411*.

(61) Stadnichuk, I. N.; Bulychev, A. A.; Lukashev, E. P.; Sinetova, M. P.; Khristin, M. S.; Johnson, M. P.; Ruban, A. V. Far-Red Light-Regulated Efficient Energy Transfer from Phycobilisomes to Photosystem i in the Red Microalga Galdieria Sulphuraria and

Photosystems-Related Heterogeneity of Phycobilisome Population. *Biochim Biophys Acta Bioenerg* **2011**, *1807* (2), 227–235. https://doi.org/10.1016/j.bbabio.2010.10.018.

(62) Marquardt, J. Effects of Carotenoid-Depletion on the Photosynthetic Apparatus of a Galdieria Sulphuraria (Rhodophyta) Strain That Retains Its Photosynthetic Apparatus in the Dark. *J Plant Physiol* **1998**, *152* (4–5), 372–380. https://doi.org/10.1016/S0176-1617(98)80250-2.

(63) Blanken, W.; Postma, P. R.; de Winter, L.; Wijffels, R. H.; Janssen, M. Predicting Microalgae Growth. *Algal Res* **2016**, *14*, 28–38. https://doi.org/10.1016/j.algal.2015.12.020.

(64) Kliphuis, A. M. J.; de Winter, L.; Vejrazka, C.; Martens, D. E.; Janssen, M.; Wijffels, R. H. Photosynthetic Efficiency of Chlorella Sorokiniana in a Turbulently Mixed Short Light-Path Photobioreactor. *Biotechnol Prog* **2010**, *26* (3), 687–696. https://doi.org/10.1002/btpr.379.

(65) Li, J.; Stamato, M.; Velliou, E.; Jeffryes, C.; Agathos, S. N. Design and Characterization of a Scalable Airlift Flat Panel Photobioreactor for Microalgae Cultivation. *J Appl Phycol* **2015**, *27* (1), 75–86. https://doi.org/10.1007/s10811-014-0335-1.

(66) Carfagna, S.; Bottone, C.; Cataletto, P. R.; Petriccione, M.; Pinto, G.; Salbitani, G.; Vona, V.; Pollio, A.; Ciniglia, C. Impact of Sulfur Starvation in Autotrophic and Heterotrophic Cultures of the Extremophilic Microalga Galdieria Phlegrea (Cyanidiophyceae). *Plant Cell Physiol* **2016**, *57* (9), 1890–1898. https://doi.org/10.1093/pcp/pcw112.

(67) Abiusi, F.; Moñino Fernández, P.; Canziani, S.; Janssen, M.; Wijffels, R. H.; Barbosa, M. Mixotrophic Cultivation of Galdieria Sulphuraria for C-Phycocyanin and Protein Production. *Algal Res* **2022**, *61*. https://doi.org/10.1016/j.algal.2021.102603.

(68) Selvaratnam, T.; Pegallapati, A. K.; Montelya, F.; Rodriguez, G.; Nirmalakhandan, N.; Van Voorhies, W.; Lammers, P. J. Evaluation of a Thermo-Tolerant Acidophilic Alga, Galdieria Sulphuraria, for Nutrient Removal from Urban Wastewaters. *Bioresour Technol* **2014**, *156*, 395–399. https://doi.org/10.1016/j.biortech.2014.01.075.

(69) Wan, M.; Wang, Z.; Zhang, Z.; Wang, J.; Li, S.; Yu, A.; Li, Y. A Novel Paradigm for the High-Efficient Production of Phycocyanin from Galdieria Sulphuraria. *Bioresour Technol* **2016**, *218*, 272–278. https://doi.org/10.1016/j.biortech.2016.06.045.

(70) Canelli, G.; Abiusi, F.; Vidal Garcia, A.; Canziani, S.; Mathys, A. Amino Acid Profile and Protein Bioaccessibility of Two Galdieria Sulphuraria Strains Cultivated Autotrophically and Mixotrophically in Pilot-Scale Photobioreactors. *Innovative Food Science and Emerging Technologies* **2023**, *84*. https://doi.org/10.1016/j.ifset.2023.103287.

FOR TABLE OF CONTENTS USE ONLY

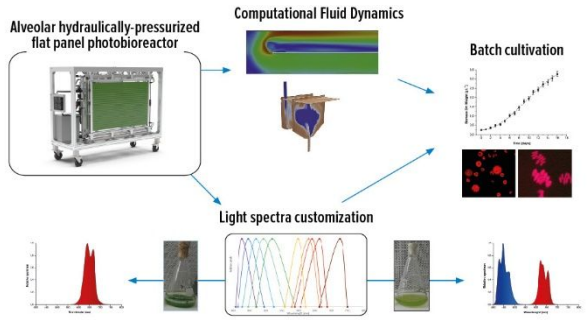

SYNOPSIS

Advanced PBR with LED lighting optimizes microalgae growth, cuts costs, enables 24h production, and aligns with sustainability principles in closed systems.